Sonochemical synthesis, structural and magnetic properties of air-stable Fe/Co alloy nanoparticles

Qiaoling Li,[ab] Hongliang Li,[a] V. G. Pol,[a] Ishai Bruckental,[c] Yuri Koltypin,[a] J. Calderon-Moreno,[d] Israel Nowik[e] and Aharon Gedanken*[a]

[a] *Department of Chemistry, Bar-Ilan University, Ramat-Gan 52900, Israel. E-mail: gedanken@mail.biu.ac.il; Fax: 972-3-5351250; Tel: 972-3-5318315*
[b] *Department of Chemistry and Engineering, North China Institute of Technology, Taiyuan 03051, China*
[c] *Department of Physics, Bar-Ilan University, Ramat-Gan 52900, Israel*
[d] *Materials and Structures Laboratory, Tokyo Institute of Technology, 4259, Nagatsuta, Midori-Ku, 226-8503, Yakohama, Japan*
[e] *Racah Institute of Physics, The Hebrew University, Jerusalem 91904, Israel*

Received* (*in Montpellier, France*) *24th February 2003, Accepted 2nd April 2003
First published as an Advance Article on the web 27th June 2003

Nanoparticles of the Fe/Co alloy have been prepared by sonolysis of a $Fe(CO)_5$ and $Co(NO)(CO)_3$ mixture in diphenylmethane solution under argon. The as-prepared product is an amorphous material having 10 nm diameter particles. Upon annealing in argon at 600 °C for 5 h, an air-stable Fe/Co alloy is formed with an increased particle size to ~40 nm. The Fe/Co alloy nanoparticles have been characterized by XRD, TEM, TGA, DSC, XPS, EPR, MES and magnetic susceptibility measurements. Materials obtained under appropriate conditions possess a very high saturation magnetization of about 150–238 emu g^{-1} and good, soft magnetic properties ($H_c = 70 - 30$ G). The nanocrystalline particles have a core-shell structure in which the iron–cobalt core is surrounded by a carbon surface layer. The stability of the nanocrystalline particle has been discussed, based on the core-shell structure.

Introduction

Recently, nanoparticles have become the focus of intensive research, owing to their numerous applications in diverse fields such as catalyst production, ultramodern electronics, optical devices, supermagnets, photographic suspensions, xerography, *etc.*[1,2] A variety of methods can be used for the formation of nanoparticles, such as molecular beam epitaxy,[3] chemical vapour deposition,[4] reduction by ionizing radiation,[5] thermal decomposition in organic solvents,[6] chemical reduction or photoreduction in reverse micelles,[7] and chemical reduction with[8] or without[9] stabilizing polymers. From all this work, it has been assessed that the particle size and the properties of nanoparticles depend strongly on the specific method of preparation and the applied experimental conditions.

The sonochemical method has been used extensively to generate novel materials with unusual properties.[10a] The chemical effects of ultrasound arise from acoustic cavitation, that is, the formation, growth, and implosive collapse of bubbles in liquid. The implosive collapse of the bubble generates a localized hot-spot through adiabatic compression or shock wave formation within the gas phase of the collapsing bubble. The conditions formed in these hotspots have been experimentally determined, with transient temperatures of *ca.* 5000 K, pressures of 1800 atm, and cooling rates in excess of 10^{10} K s^{-1}. These extreme conditions attained during bubble collapse have been exploited to decompose the metal–carbonyl bonds and generate metals,[10b–e] metal carbides,[10f] and metal oxides.[10g,h]

A protective layer on the surface of the particles prevents interaction between closely spaced magnetic bits and provides oxidation resistance.[11] Coated or air-stable Fe/Co alloy nanoparticles are of particular interest since the ferromagnetic alloys containing Fe and Co have excellent soft magnetic properties equivalent or superior to those of conventional materials, and are being used in perpendicular magnetic recording, highly sensitive magnetic sensors, toners, imaging reagents, and magnetic carriers. One of the first methods to be used to prepare metal or alloy nanoparticles was metal vapour synthesis. It has been studied extensively and is still being used. Furthermore, carbon formation has been attributed to metal carbide formation, followed by thermal decomposition of the carbide to form surface graphite and a metal core.[12a,b,c]

Amorphous Fe/Co nanoparticles were prepared by the sonolysis of $Fe(CO)_5$ and $Co(NO)(CO)_3$ in decane at 0 °C,[13] but the product was not air-stable. In the present paper, we report on a sonochemical method for the preparation of air-stable Fe/Co alloy nanoparticles by sonolysis of $Fe(CO)_5$ and $Co(NO)(CO)_3$ in diphenylmethane (DPhM), followed by the thermal treatment of the as-prepared material under argon. The nanoparticles of the air-stable Fe/Co alloy consist of a metal alloy core and a coated shell. These Fe/Co alloy nanoparticles show an excellent magnetic performance and storage stability. It is believed that the magnetic properties of Fe/Co nanocrystalline particles can be tailored to meet the requirements of various specific applications. Recently, Nikitenko *et al.* synthesized highly magnetic, air stable iron nanoparticles[14] by using power ultrasound. This study extends Nikitenko's work to the formation of an alloy, and is an extension of the previous work.

Experimental section

Diphenylmethane (DPhM) (>99%, Fluka), $Fe(CO)_5$ (99.5% STREM), and $Co(NO)(CO)_3$ were used without additional

 DOI: 10.1039/b302136j

purification. A $Fe(CO)_5$ and $Co(NO)(CO)_3$ solution of desired concentration in DPhM was sonicated in the presence of argon by means of a Sonics and Materials ultrasonic device with a direct immersion titanium horn (working frequency 20 kHz, electric power of generator 600 W, irradiation surface area of the horn 1 cm^2). The volume of the sonicated solution was 120 mL. The absorbed acoustic power, measured by the thermal probe method,[15] was found to be equal to 0.45 W mL^{-1}. In a typical preparation of a $Fe_{40}Co_{60}$ alloy, 2.0 mL $Fe(CO)_5$ (~0.15 $mol{\cdot}L^{-1}$) and 1.5 mL $Co(NO)(C)_3$ (~0.15 $mol{\cdot}L^{-1}$) were dissolved in 100 ml DPhM. The sonolysis of the solution was performed for 3 h at 20–30 °C under argon atmosphere. The temperature was maintained during sonication by a Julabo FT 901 cooler. The black solid product was separated by centrifugation, washed three times with pentane inside the N_2-filled glove box, and dried under vacuum at room temperature. The annealing of the solids was performed under an argon flow (99.996%) for 5 h at 600 °C, yielding ~60% $Fe_{40}Co_{60}$ alloy by weight.

XRD was recorded on a Bruker AXS D* Advanced Powder X-ray Diffractometer (Cu-K_α radiation, $\lambda = 0.15418$ nm). The XRD diffraction patterns of the as-prepared material were measured in a tightly closed cell, which was closed in a nitrogen filled glove box to avoid sample contact with air. Measurements of annealed samples were performed without special precautions. Low resolution TEM was obtained with a JEOL-JEM100SX electron microscope with 80–100 kV accelerating voltage. Energy-dispersive X-ray (EDX) analysis was measured on a JEOL-JSM-840 scanning microscope. Magnetic measurements were performed at room temperature using a Quantum Design MPMS SQUID magnetometer. The thermogravimetric (TGA) and differential scanning calorimetric analyses (DSC) were performed by using Mettler Toledo TGA/SDTA 851 and DSC-25/TC-15 devices, respectively, under pure nitrogen flow. X-ray photoelectron spectroscopy (XPS) was recorded using an AXIA, HIS 165, ULTRA (Krato Analytical) device. The XPS data were acquired for $Fe_{2p,}$ $Co_{2p,}$ C_{1s}, and O_{1s} photoelectron emission. Elemental analysis was carried out by an Eager 2000 CHN analyzer. Mössbauer effect spectroscopy (MES) studies were performed using a ^{57}Co:Rh source (50 mCi) and a conventional constant acceleration Mössbauer drive. The samples for XRD, TGA, DSC, EPR, and magnetic susceptibility measurements were prepared in an inert atmosphere of a nitrogen glove box.

Results and discussion

We have noticed that the sonochemical efficiency for decomposition of $Co(NO)(CO)_3$ is less than for $Fe(CO)_5$, so it is necessary to use an initial excess of $Co(NO)(CO)_3$ to obtain the required alloy composition. The poor reactivity of $Co(NO)(CO)_3$ can be traced to its lower vapour pressure when compared with $Fe(CO)_5$. As the precursor's vapour pressure increases, its concentration in the bubble (*i.e.*, the gas phase within the collapsing cavity) increases linearly, thus increasing the observed sonochemical reaction rate. Fe_xCo_y is termed as the respective composition obtained in the product.

XRD measurements

The X-ray diffraction (XRD) for the as-prepared sample of $Fe_{40}Co_{60}$ is shown in Fig. 1. The amorphous nature of the alloy is demonstrated by the absence of any diffraction peaks. Fig. 2 shows the XRD patterns for samples of the $Fe_{40}Co_{60}$ alloy annealed at different atmosphere and temperatures. Fig. 2a shows the XRD pattern for the sample annealed at 500 °C for 5 h under an argon atmosphere. The pattern does not show well-defined peaks characteristic of a crystalline material. This means that 500 °C is not sufficient to crystallize

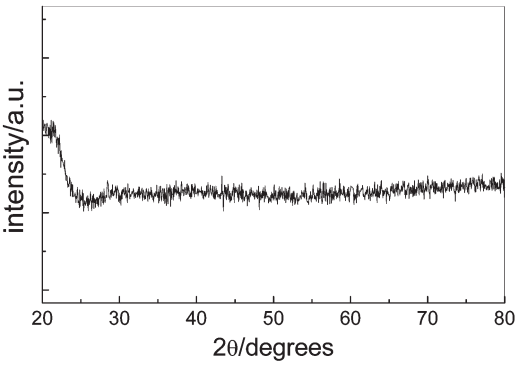

Fig. 1 XRD pattern of amorphous $Fe_{40}Co_{60}$.

this alloy. Fig. 2b shows the XRD pattern for the sample annealed at 600 °C for 5 h under argon. The pattern was dominated by bcc Fe/Co. No peaks attributable to iron/cobalt oxide or other iron/cobalt impurity phases are observed. Fig. 2c shows the XRD pattern for the sample annealed at 600 °C for 5 h in air. The pattern showed strong and relatively broadened peaks corresponding to $CoFe_2O_4$. The broadening of the $CoFe_2O_4$ peaks may be due to the small grain size. The Co:Fe atomic ratio in the oxidized ferrite is very different from their ratio in the alloy. This is perhaps due to the partial conversion of the Co to Co_2O_3 whose diffraction peaks might be beneath those of $CoFe_2O_4$. The presence of the Fe/Co alloy could not be observed due to the formation of cobalt ferrite during the annealing process in air atmosphere.

The diffraction patterns for the materials (annealed under pure argon at 600 °C for 5 h) containing from 30 to 70 at.% cobalt are the same as $Fe_{40}Co_{60}$, and correspond to a body-centered-cubic crystal. No ordered α' phase has been detected. All the alloys that we have tested so far crystallize in the bcc structure, which is consistent with the known Fe/Co equilibrium phase diagram.[16,17] Furthermore, the lattice constants for all compositions studied were about the same. It is clear from the XRD patterns that the particles are not a mixture of pure iron and pure cobalt, but a binary alloy of iron and cobalt atoms. The fine diffraction lines and the lack of background show that the very well crystallized single phase of the alloy was obtained. To obtain more quantitative information, the Debye–Scherrer formula[18]

$$L = 0.9\lambda/(B \times \cos(\theta)) \quad (1)$$

has been applied to calculate the size of the crystalline alloy nanocrystals, where L is the coherence length, B is the full

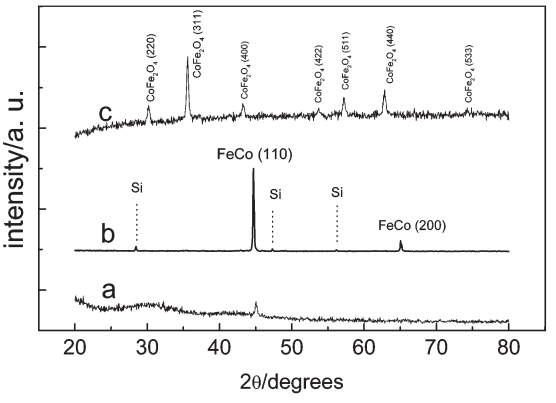

Fig. 2 XRD patterns of $Fe_{40}Co_{60}$ annealed with different conditions: (a) annealed at 500 °C under argon; (b) annealed at 600 °C under argon; (c) annealed at 600 °C in air. (The dotted lines show the peaks of silicon internal standard).

width at half maximum (fwhm) of the peak, λ is the wavelength of the X-ray radiation, and θ is the angle of diffraction. In the case of spherical crystallites, the relation between L and D, the diameter of the crystallite, is given as $L = {}^3/_4 D$. The value of L obtained for the $Fe_{40}Co_{60}$crystalline particle is 31 nm. This translates to a crystallite size of 41 nm, which is close to the following TEM results.

Mössbauer spectroscopy measurements

Three samples annealed at 500 °C, 550 °C and 600 °C have been measured. The spectra at room temperature are shown in Fig. 3. One observes that while samples (a) and (b) exhibit the presence of foreign phases, probably Fe_3O_4, sample (c) is a pure single Fe–Co alloy phase. The hyperfine interaction parameters for sample (c) are; isomer shift zero relative to pure iron, quadrupole interaction zero like in pure iron, but magnetic hyperfine field of 355 kOe, 10% larger than in iron.

Elemental and EDX analysis

Alloy compositions were determined by elemental and energy-dispersive X-ray (EDX) analysis. The presence and ratio of Fe and Co were examined by EDX measurements. The quantitative values of the Fe and Co ratio were measured for the annealed product. The elemental analysis of the amorphous sample could not be done due to the burning of the sample in air atmosphere. The elemental analysis of the annealed samples showed that the alloy powders have over 97% metal by mass, with small amounts of carbon ($< 2\%$) and hydrogen ($< 0.5\%$). The presence of carbon and hydrogen is presumably the result of the decomposition of DPhM solvents[14] or CO adsorbed during ultrasonication.

TEM measurements

The transmission electron microscope (TEM) image (Fig. 4a) of the as-prepared $Fe_{40}Co_{60}$ sample shows the alloy powder as agglomerates of small particles with average diameters of 20 nm. The exact size of the particle is difficult to determine as most of the particles are aggregated in a sponge-like form. The electron diffraction (Fig. 4b) of the alloy particles shows only a diffuse ring characteristic of amorphous materials. The TEM micrograph of the annealed $Fe_{40}Co_{60}$ sample (heated at 600 °C for 5 h under Ar) is shown in Fig. 5a. The near-spherical particles of 20–40 nm can be seen in this micrograph. The ED pattern in Fig. 5b indicates that these particles

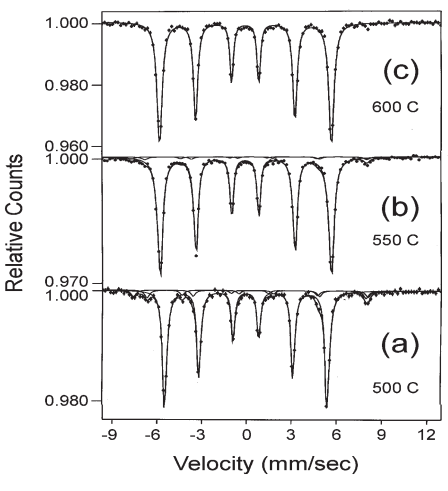

Fig. 3 Mössbauer spectra at room temperature of samples annealed at 500 °C, at 550 °C, and at 600 °C.

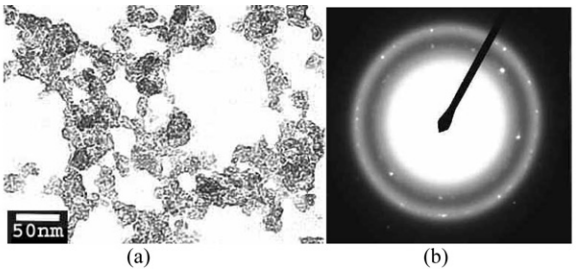

Fig. 4 (a) TEM images of the as-prepared $Fe_{40}Co_{60}$ and (b) its SAED.

are polycrystalline. The amorphous disordered aggregated particles are converted into near-spherical particles during the annealing process.

Thermal analysis

Thermal analysis was carried out by using TGA and DSC measurements. Fig. 6 shows TGA curves of the sample $Fe_{40}Co_{60}$ for as-prepared and annealed samples. The TGA curve (Fig. 6a) exhibits a three-stage mass loss at 100–230 °C, 250–450 °C, and 760–900 °C of about 14.4 wt.%, 8.3 wt.%, and 10.7 wt,%, respectively. This total 33.4% weight loss corresponds to the loss of organic impurities which were formed on the surface of $Fe_{40}Co_{60}$ alloy nanoparticles during the sonolytic decomposition of diphenylmethane.[14] Indeed, this loss, occurring in three steps, could be associated with complete decomposition of C–H bonds and the release of hydrogen at different temperatures. In order to study the stability of an annealed sample (600 °C for 5 h) in air atmosphere, we have carried out the thermogravimetric analysis of this sample. Fig. 6b shows that the annealed sample $Fe_{40}Co_{60}$ has good stability against oxidation below 350 °C, due to the formation of a carbon protective shell on the surface of the alloy nanoparticles during the annealing process.

The differential scanning calorimetric (DSC) curves of the as-prepared amorphous $Fe_{40}Co_{60}$ sample are shown in Fig. 7. A wide endothermic peak below 280 °C, centered around 216 °C, can be seen in the DSC curve. It indicates the decomposition of the adsorbed surface organic impurities. The impurities are supposed to be related to the organic sonopolymer thermolysis.[14] The $Fe_{40}Co_{60}$ sample shows a wide exothermic peak centered around 500 °C, which corresponds to the phase change from amorphous to crystalline. The broad exotherm could be explained as being due to the wide size distribution of the alloy nanoparticles. Indeed, the sample annealed at 500 °C for 5 h was not well crystallized, confirmed by XRD measurements (Fig. 2a). On the other hand, the sample annealed at 600 °C (where exotherm ends) shows well-defined peaks in the XRD measurements, characteristic of the complete crystallization of the alloy particles. After cooling and a second heating cycle, the DSC curve was featureless (data not shown).

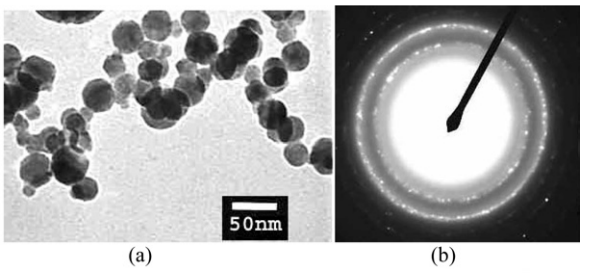

Fig. 5 (a) TEM images of $Fe_{40}Co_{60}$ annealed at 600 °C for 5 h; (b) its micro-diffraction pattern.

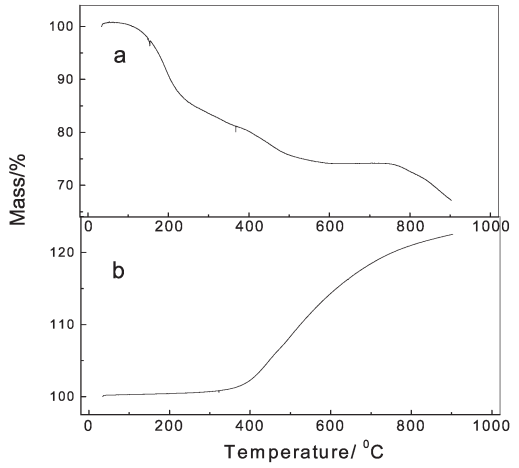

Fig. 6 TGA curves for $Fe_{40}Co_{60}$ samples: (a) as-prepared sample (under nitrogen flow), (b) crystalline sample (under air atmosphere).

Magnetic measurements

The magnetic properties were investigated by magnetic susceptibility and an electron spin resonance method. The magnetization *vs.* magnetic field curves for the as-prepared and annealed alloy samples are shown in Figs. 8a and 8b–e, respectively. The specific saturation magnetization M_s and coercivity H_c are calculated for the different ferromagnetic compositions of the alloys. The magnetization curve of the amorphous sample $Fe_{40}Co_{60}$ measured at room temperature (Fig. 8a) does not reach saturation even at a magnetic field of 15 kG, and no hysteresis is found, indicating that the as-prepared (amorphous) Fe/Co particles are superparamagnetic. Shafi *et al.* also reported a similar behavior.[19]

Higher saturation magnetizations than those in Fig. 8a were observed in Figs. 8b–e, because of the crystalline nature of the compounds. In the case of the crystalline $Fe_{40}Co_{60}$ alloy, the saturation magnetization and coercivity are 238 emu g^{-1} and 73 Oe, respectively. These numbers were higher than those obtained for other compositions. Crystalline alloys show very high saturation magnetization (Figs. 8b–e) ranging from 150 emu g^{-1} to 238 emu g^{-1}. These saturation magnetization and coercivity numbers are close to the reported data of air-stable iron nanoparticles, which show saturation magnetization of 212 emu g^{-1} and coercivity of 40 Oe,[14] respectively. The difference in the magnetic properties in different stoichiometries or compositions can be explained as due to the interaction of the magnetic moments in the Fe/Co alloys.[20]

Since the coercivity of the Fe/Co particles mainly originates from the crystal and shape anisotropy, the low coercivity in the as-prepared alloy can be attributed to the low magnetic anisotropy of the spherical Fe/Co alloy nanoparticles, which contain nanoparticles smaller (20–40 nm) than the critical diameter, D_c, of the corresponding Fe/Co alloy.[21]

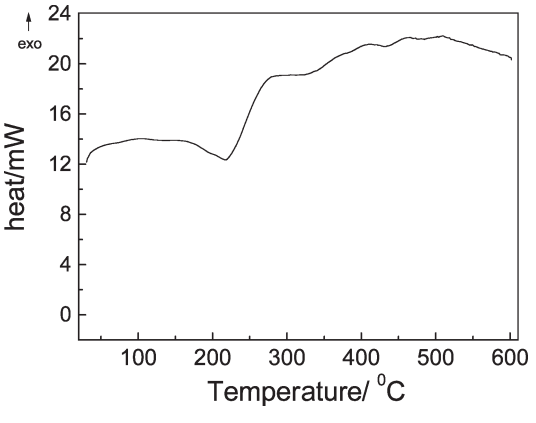

Fig. 7 DSC curve of as-prepared amorphous $Fe_{40}Co_{60}$ sample.

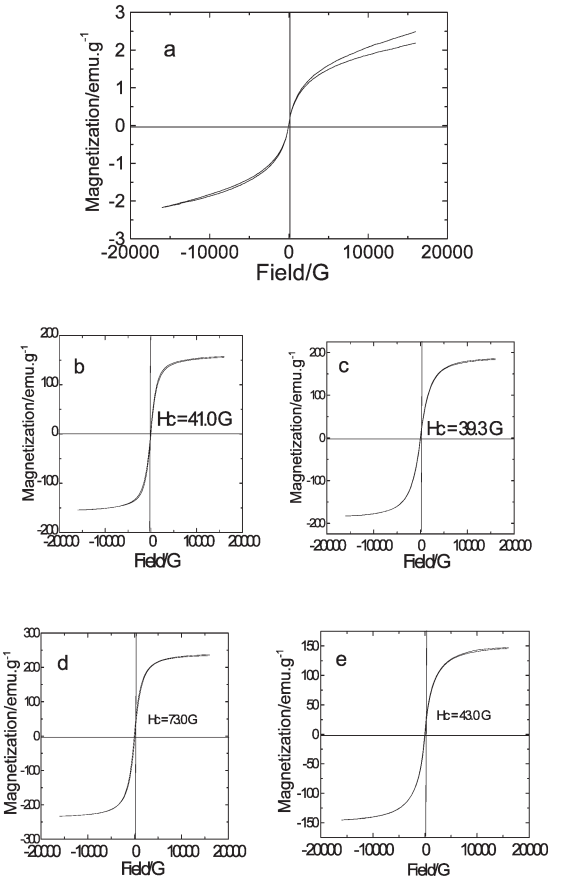

Fig. 8 Room-temperature magnetization curves of Fe/Co samples: (a) amorphous $Fe_{40}Co_{60}$, (b) annealed $Fe_{30}Co_{70}$, (c) annealed $Fe_{50}Co_{50}$, (d) annealed $Fe_{40}Co_{60}$, (e) annealed $Fe_{70}Co_{30}$.

Our measured coercivity is much smaller than the high coercivity of about 1780 Oe, which was obtained for the $CoFe_2$ nanoparticles.[22] It has also been reported that the presence of an oxide can be the cause for enhancing the resulting coercivity.[23,24] A change of the coercivity of Fe or Co nanoparticles from a few tens to a few hundred Oe has been observed when the nanoparticles were oxidized.[24,25] On the other hand, our low coercivity is close to the reported coercivity of a few tens of Oe of Fe and Co nanoparticles, which are in contact with non-oxidized agents.[22,23] In the light of this comparison, the measured coercivity data is, on the one hand, consistent with other reports and, on the other hand, with the surface properties resulting from other measurements. (See the EDAX, the XPS and the HRTEM results.)

Electron paramagnetic resonance is a powerful technique for studying the microstructure and the electronic properties of the sample. EPR spectra of the amorphous and annealed alloy Fe/Co nanoparticles were measured at 300 K. The EPR spectrum (Fig. 9a) of the amorphous sample with Gaussian shape is centered at $g = 2.2858$ and has a peak-to-peak separation (ΔH_{pp}) of 1600 G. The broad paramagnetic resonance signal can be associated with the paramagnetic nature of the alloy particles. The broadening of the EPR line arises from strong interparticle dipolar interactions that provide an effective spin relaxation mechanism.[26] The crystalline sample annealed at 600 °C was highly ferromagnetic and a resonance spectrum could not be recorded under identical conditions, even with small amounts of the sample measured (Fig. 9b).

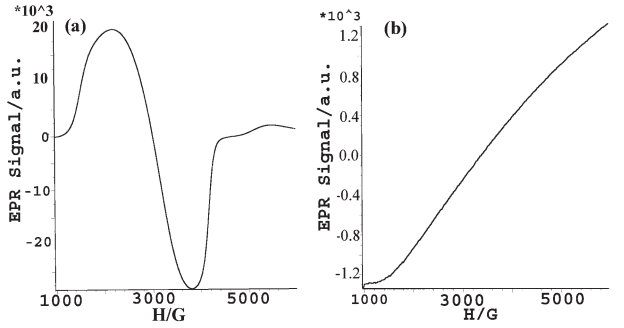

Fig. 9 EPR spectra of the $Fe_{40}Co_{60}$ nanoparticles: (a) amorphous, (b) crystalline.

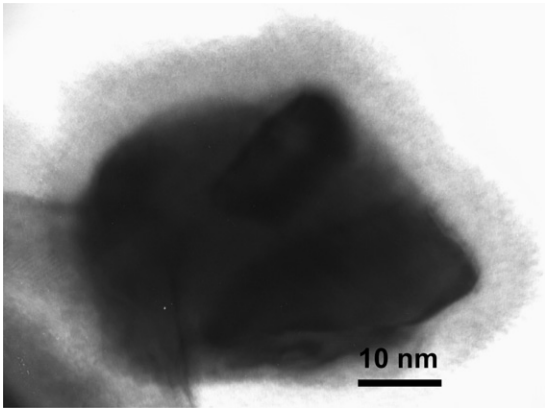

Fig. 10 HRTEM of a $Fe_{40}Co_{60}$ particle annealed at 600 °C.

XPS and HRTEM measurements

Indeed, we did not observe any carbon diffraction peaks in the XRD patterns due to its amorphous nature. In order to study the presence of carbon, which acts as a protective shell in the annealed particles, we have carried out XPS and HRTEM measurements. XPS is a very sensitive technique for analysing the surface composition of the particles. The results of the surface analysis of the alloy and the composition of Fe, Co, O and C are shown in Table 1. The amorphous alloy ($Fe_{40}Co_{60}$), when annealed in air, shows a high concentration of Fe, Co and O compared with the sample annealed in an argon atmosphere. On the other hand, the sample annealed under argon shows a very high concentration of carbon (around three times) compared with the sample annealed in air. These results can be explained as follows: after annealing in an argon atmosphere, the surface of the alloy particle is covered with carbon (>68 at.%). The sample that was annealed in air has undergone oxidation, resulting in CO_2, which reduces the concentration of carbon on the particle's surface. This is evidenced by the presence of more than 56% of oxygen, while the concentration of carbon is only around 21%. This indicates that the protective shell of carbon was formed during the annealing of the alloy in an inert atmosphere. The surface composition of the $Fe_{40}Co_{60}$ alloy demonstrates some enrichment of Fe over Co. Similar results of an iron-enriched surface have been reported by other researchers using other preparation methods.[27] High resolution TEM measurements have been carried out to confirm the presence of the proactive shell. The HRTEM image of particles annealed at 600 °C is depicted in Fig. 10. The protective carbon layer is distinctive. The carbon layer is amorphous and it varies in thickness in the range 5–10 nm.

Particle stability

The as-prepared material is pyrophoric and must be handled in an inert atmosphere. On the other hand, the annealed materials do not show visible changes in colour, shape, structure, or magnetism when stored at room temperature in air. The time-stability of the nanocrystalline particles obtained was tested by sequential measurements of XRD and magnetization values. It was observed that the samples annealed at 600 °C exhibit a strong resistance to oxidation. The XRD spectra and Ms values do not change after at least 5 months of contact with air.

The annealed particles are also stable for at least one week upon contact with water, an 0.5 M NaOH solution, or ethanol. We attribute the particle stability to the protective shell of carbon formed during annealing. Usually, iron and cobalt are very sensitive to oxygen in air and are easily oxidized. By analysing XRD, element analysis and XPS results, we conclude that the Fe/Co alloy nanoparticles were covered with a protective layer mainly composed of carbon. The mechanism of the formation of this structure will be discussed in the following section.

Table 1 XPS measurements of Fe, Co, C, and O surface concentrations for annealed samples using Fe2p (711.5 eV), Co2p (780.1 eV), C1s (284.35 eV), and O1s (530.1 eV) signals respectively

	Surface concentration/at.%			
Sample $Fe_{40}Co_{60}$	Fe	Co	C	O
Annealed in air	12.80	8.89	21.77	56.55
Annealed under argon	2.70	1.67	68.16	27.47

Proposed mechanism

The chemical reactions driven by intense ultrasonic waves strong enough to produce cavitation are oxidation, reduction, dissolution, and decomposition.[10a,28–31] Other reactions, such as promotion of polymerisation, have also been reported to be induced by ultrasound. It is known that three different regions are formed[32] during the DPhM solution's sonochemical process: (a) The inner environment of the collapsing bubble, where elevated temperatures (several thousands of degrees) and pressures (hundreds of atmospheres) are produced. A gas phase reaction occurs in this region. (b) The interfacial region where the temperature is lower than in the gas-phase region, but still high enough to induce a sonochemical liquid phase reaction. (c) The bulk solution, which is at ambient conditions. It is believed that the decomposition of the carbonyls occurs inside the collapsing bubble, while the decomposition of the DPhM and the formation of the polymer takes place in the interface region. This is due to the volatility of the carbonyls and the non-volatility of the DPhM. This will also explain why the polymer wraps around the alloyic core, and, after annealing, forms the protective shell layer. The amorphicity of the alloy also indicates that the reaction occurs inside the collapsing bubble, since the extreme cooling rates ($>10^{11}$ K s^{-1}) obtained are responsible for the creation of amorphous products.[33] Unlike sonochemical reactions involving two metallic salts,[34] which occur in the interface region and lead to a core-shell structure, the formation of an homogeneous alloy indicates that the decomposition rate of the two carbonyls is of the same speed. After annealing at high temperature in an inert atmosphere, the adsorbed organic materials can react with the metal to form a carbide intermediate, which then decomposes at high temperature, forming the carbon protective shell *in vivo*, which prevents the Fe/Co alloy core from oxidation by air.[35]

Conclusions

Sonochemical decomposition of the solutions of volatile organic precursors, $Co(NO)(CO)_3$ and $Fe(CO)_5$, in diphenylmethane (DPhM) at 293–300 K, under an argon atmosphere, yielded pyrophoric amorphous Fe/Co alloy nanoparticles. Annealing of the as-prepared material in argon at 600 °C leads to the growth of the Fe/Co particle size, forming air-stable nanocrystalline Fe/Co particles due to the carbon coating on the surface of the alloy nanoparticles. A very high saturation magnetization was observed for the $Fe_{40}Co60$ alloy composition (238 emu g−1). This high Ms is achieved due to the alloy that has a protective carbon shell to avoid oxidation.

Acknowledgements

Dr Q. L. Li thanks the Kort 100 Scholarship Foundation for supporting her postdoctoral fellowship. Dr H. L. Li thanks the Bar-Ilan Research Authority for a postdoctoral fellowship. A. Gedanken also thanks the BMBF, Germany, for financial support through the Energy Program.

References

1 G. C. Bond, *Surf. Sci.*, 1985, **156**, 966.
2 (*a*) H. Weller, *Angew. Chem., Int. Ed. Engl.*, 1993, **32**, 41; (*b*) G. Schmidt, *Chem. Rev.*, 1992, **92**, 1709; (*c*) L. N. Lewis, *Chem. Rev.*, 1993, **93**, 2693.
3 D. W. Bahnemann, *Isr. J. Chem.*, 1993, **33**, 115.
4 N. Satoh and K. Kimura, *Bull. Chem. Soc. Jpn.*, 1989, **62**, 1758.
5 A. Henglein, *J. Phys. Chem.*, 1993, **97**, 5457.
6 K. Esumi, T. Tano, K. Torigoe and K. Meguro, *Chem. Mater.*, 1990, **2**, 564.
7 M. P. Pileni, I. Lisiecki, L. Motte, C. Petit, J. Cizeron, N. Moumen and P. Lixon, *Prog. Colloid Polym. Sci.*, 1993, **93**, 1.
8 N. Toshima, T. Yonezawa and K. Kushihashi, *J. Chem. Soc., Faraday Trans.*, 1993, **89**, 2537.
9 L. M. Liz-Marzan and A. P. Philipse, *J. Phys. Chem.*, 1995, **99**, 15 120.
10 (*a*) *Ultrasound: Its Chemical, Physical and Biological Effects*, ed. K. S. Suslick, VCH, Weinheim, 1988; (*b*) K. S. Suslick, S. B. Choe, A. A. Cichowlas and M. W. Grinstaff, *Nature*, 1991, **353**, 414; (*c*) Yu. Koltypin, G. Katabi, R. Prozorov and A. Gedanken, *J. Non-Cryst. Solids*, 1996, **201**, 159; (*d*) Y. Nagata, Y. Mizukoshi, K. Okitsu and Y. Maeda, *Radiat. Res.*, 1996, **146**, 333; (*e*) K. Okitsu, Y. Mizukoshi, H. Bandow, Y. Maeda, T. Yamamoto and Y. Nagata, *Ultrason. Sonochem.*, 1996, **3**, S249; (*f*) T. Hyeon, M. Fang and K. S. Suslick, *J. Am. Chem. Soc.*, 1996, **118**, 5492; (*g*) X. Cao, Yu. Koltypin, G. Katabi, I. Felner and A. Gedanken, *J. Mater. Res.*, 1997, **12**, 405; (*h*) N. Arul Dhas and A. Gedanken, *J. Phys. Chem. B*, 1997, **10**, 9495.
11 P. J. F. Harris, *Carbon Nanotubes and Related Structures*, Cambridge University Press, New York, 1999.
12 (*a*) K. J. Klabunde, *Chemistry of Free Atoms and Particles*, Academic Press, New York, 1980; (*b*) K. J. Klabunde, *Free Atoms and Nanoparticles*, Academic Press, San Diego, 1994; K. J. Klabunde, ed., *Nanoscale Chemistry of Nanoscale Materials*, Wiley Interscience, New York, 2001.
13 K. Suslick, T. Hyeon, M. Fang and A. A. Cichowlas, *Mater. Sci. Eng. A*, 1995, **204**, 186.
14 S. I. Nikitenko, Y. Koltypin, O. Palchik, I. Felner, X. N. Xu and A. Gedanken, *Angew. Chem. Int. Ed.*, 2001, **40**, 23.
15 *Chemistry with Ultrasound*, ed. T. J. Mason, Elsevier, New York, 1994.
16 B. D. Cullity, *Introduction to Magnetic Materials*, Addison-Wesley, NY, 1972, 146.
17 T. Nishizawa and K. Ishida, *Bull. Alloy Phase Diagram*, 1984, 250.
18 A. Guinier, *X-ray Diffraction*, Freeman, San Francisco, CA, 1963.
19 K. V. P. M. Shafi, A. Gedanken and R. Prozorov, *J. Mater. Chem.*, 1998, **8**(3), 769.
20 Y. D. Kim, J. Y. Chung, J. Kim and H. Jeon, *Mater. Sci. Eng. A*, 2000, **291**, 17.
21 D. L. Leslie-Pelecky and R. D. Rieke, *Chem. Mater.*, 1996, **8**, 1770.
22 Y. D. Yao, Y. Y. Chen, S. F. Lee, W. C. Chang and H. L. Hu, *J. Magn. Magn. Mater.*, 2002, **239**, 249.
23 S. Gangopadhyay, G. C. Hadjipanayis, B. Dale, C. M. Sorensen, K. J. Klabunde, V. Papaefthymiou and A. Kostikas, *Phys. Rev. B*, 1992, **45**, 9778.
24 A. Tsoukatos, H. Wan, G. C. Hadjipanayis, V. Papaefthymiou, A. Kostikas and A. Simopoulos, *J. Appl. Phys.*, 1993, **73**, 6967.
25 A. S. Edelstein, B. N. Das, R. L. Holtz, N. C. Koon, M. Rubinstein, S. A. Wolf and K. E. Kihlstrom, *J. Appl. Phys.*, 1987, **61**, 3320.
26 V. K. Sharma and F. Waldner, *J. Appl. Phys.*, 1977, **48**, 4298.
27 M. Nakamura, B. J. Wood, P. Y. Hou, H. Wise, in *Proc. Int. Congr. Catal.*, Tokyo, Kodansha Ltd., Tokyo, 1987.
28 A. E. Alegria, Y. Lion, T. Kondo and P. Riesz, *J. Phys. Chem.*, 1989, **93**, 4908.
29 M. Gutierrez and A. Henglein, *J. Phys. Chem.*, 1988, **92**, 2978.
30 J. Z. Sostaric, P. Mulvaney and F. Grieser, *J. Chem. Soc., Faraday Trans.*, 1995, **91**, 2843.
31 M. Gutierrez, A. Henglein and J. Dohrmann, *J. Phys. Chem.*, 1987, **91**, 6687.
32 (*a*) K. S. Suslick and D. A. Hammerton, *IEEE Trans. Sonics Ultrason.*, 1986, **143**, SU–33; (*b*) K. S. Suslick and D. A. Hammerton, *Ultrasonics Int.*, 1985, 231; (*c*) K. S. Suslick, R. E. Cline and D. A. Hammerton, *Ultrason. Symp. Proc.*, 1985, **2**, 1116.
33 P. Jeevanandam, Y. Koltypin, A. Gedanken and Y. Mastai, *J. Mater. Chem.*, 2000, **10**, 511.
34 R. Oshima, T. A. Yamamoto, Y. Mizukoshi, Y. Nagata and Y. Maeda, *Nanostruct. Mater.*, 1999, **12**, 111.
35 P. Hooker, B. J. Tan, K. J. Klabunde and S. Suib, *Chem. Mater.*, 1991, **3**, 947.